

---

# TRAINING NORMALIZING FLOWS FROM DEPENDENT DATA

**Matthias Kirchler**  
Hasso Plattner Institute  
TU Kaiserslautern

**Christoph Lippert**  
Hasso Plattner Institute  
Hasso Plattner Institute for  
Digital Health at Mount Sinai

**Marius Kloft**  
TU Kaiserslautern

## ABSTRACT

Normalizing flows are powerful non-parametric statistical models that function as a hybrid between density estimators and generative models. Current learning algorithms for normalizing flows assume that data points are sampled independently, an assumption that is frequently violated in practice, which may lead to erroneous density estimation and data generation. We propose a likelihood objective of normalizing flows incorporating dependencies between the data points, for which we derive a flexible and efficient learning algorithm suitable for different dependency structures. We show that respecting dependencies between observations can improve empirical results on both synthetic and real-world data.

## 1 INTRODUCTION

Density estimation and generative modeling of complex distributions are fundamental problems in statistics and machine learning and significant in various application domains. Remarkably, normalizing flows (Rezende & Mohamed, 2015; Papamakarios et al., 2021) can solve both of these tasks at the same time. Furthermore, their neural architecture allows them to capture even very high-dimensional and complex structured data (such as images and time series). In contrast to other deep generative models such as variational autoencoders (VAEs), which only optimize a lower bound on the likelihood objective, normalizing flows optimize the likelihood directly.

Previous work on both generative models and density estimation with deep learning assumes that data points are sampled *independently* from the underlying distribution. However, this modelling assumption is oftentimes heavily violated in practice. Figure 1 illustrates why this can be problematic. A standard normalizing flow trained on dependent data will misinterpret the sampling distortions in the training data as true signal (Figure 1c). Our proposed method, on the other hand, can correct for the data dependencies and reconstruct the original density more faithfully (Figure 1d).

The problem of correlated data is very common and occurs in many applications. In the biomedical domain, large cohort studies (such as the UK Biobank (Bycroft et al., 2018)) involve participants that oftentimes are directly related (such as parents and children) or indirectly related (by sharing genetic material due to a shared ancestry)—a phenomenon called population stratification (Cardon & Palmer, 2003). These dependencies between individuals play a major role in the traditional analyses of these data and require sophisticated statistical treatment (Lippert et al., 2011). Other biomedical applications include longitudinal studies with repeat measurements for individuals.

In finance, accurate density estimation and modeling of assets (e.g., stock market data) is essential for risk management and modern trading strategies. Data points are often heavily correlated with one another, due to time, sector, or other relations. Traditionally, financial analysts often use copulas for the modeling of non-parametric data, which themselves can be interpreted as a simplified version of normalizing flows (Papamakarios et al., 2021). Copulas commonly in use, however, are limited in their expressivity, which has led some authors even to blame the 2007-2008 global financial crisis on the use of inadequate copulas (Salmon, 2009). Many more examples appear in other settings, such as data with geospatial dependencies, as well as in time series and video data, or repeat measurements in image data.

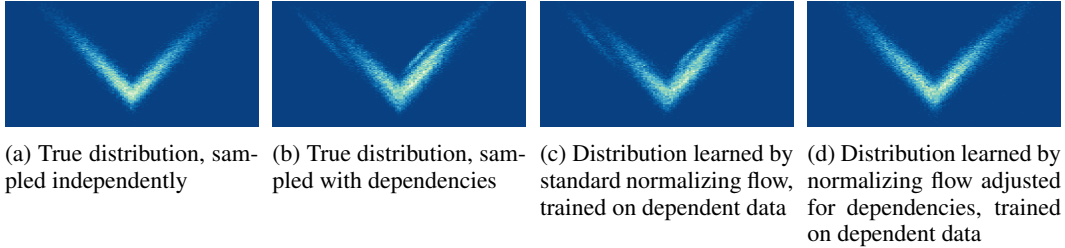


Figure 1: Example setting with synthetic data sampled with inter-instance dependencies. Training a standard normalizing flow on this data biases the model. Adjusting for the dependencies during training recovers the true underlying distribution.

In certain settings from classical parametric statistics, direct modeling of the dependencies in maximum likelihood models is analytically feasible. For linear and generalized linear models, dependencies are usually addressed either with random effects in linear mixed models (Jiang & Nguyen, 2007) or sometimes only by the inclusion of fixed-effects covariates into the models (Price et al., 2006). Recent work in deep learning introduced concepts from random effects linear models into deep learning for *prediction* tasks such as regression and classification (Simchoni & Rosset, 2021; Xiong et al., 2019; Tran et al., 2020). In federated learning of generative models, researchers usually deal with the break of the non-i.i.d. assumptions with ad hoc methods and without consideration of the statistical implications (Augenstein et al., 2020; Rasouli et al., 2020). These methods also only consider block-type, repeat-measurement dependencies for multi-source integration. To the best of our knowledge, both deep generative models and deep density estimation so far lack the tools to address violations against the independence assumption in the general setting and in a well-founded statistical framework.

In this work we show that the likelihood objective of normalizing flows naturally allows for the explicit incorporation of data dependencies. We investigate several modes of modeling the dependency between data points, appropriate in different settings. We also propose efficient optimization procedures for this objective. Finally, we apply our proposed method to several synthetic and real-world data sets, showing that adjustment for dependencies can significantly improve the model fit of normalizing flows.

## 2 METHODS

In this section we describe our methodology for training normalizing flows from dependent data. First, we will derive a general formulation of the likelihood under weak assumptions on the dependencies among observations. Afterwards, we will investigate two common settings in more detail.

### 2.1 BACKGROUND: LIKELIHOOD WITH INDEPENDENT OBSERVATIONS

A normalizing flow is an invertible function  $t : \mathbb{R}^p \rightarrow \mathbb{R}^p$  that maps a  $p$ -dimensional noise variable  $u$  to a  $p$ -dimensional synthetic data variable  $x$ . The noise variable  $u$  is usually distributed following a simple distribution (such as a  $\mathcal{N}_p(0, I_p)$  or  $\mathcal{U}_{[0,1]^p}$ ), for which the density is explicitly known and efficiently computable. By using the change of variable formula, the log-density can be explicitly computed as

$$\log(p_x(x)) = \log(p_u(u)) - \log(|\det J_t(u)|),$$

where  $u := t^{-1}(x)$  and  $J_t(u)$  is the Jacobian matrix of  $t$  in  $u$ .

Given a data set  $x_1, \dots, x_n$ , if the observations are **independent** and identically distributed, the full log-likelihood function readily factorizes into its respective marginal densities:

$$\log(p_x(x_1, \dots, x_n)) = \sum_{i=1}^n \log(p_x(x_i)) = \sum_{i=1}^n \log(p_u(u_i)) - \log(|\det J_t(u_i)|).$$

The function  $t$  is usually chosen in such a way that both the inverse  $t^{-1}$  and the determinant of the Jacobian  $J_t$  can be efficiently evaluated, e.g. using coupling layers (Dinh et al., 2017). Therefore,

all of the terms in the likelihood can be explicitly and efficiently computed and the likelihood serves as the direct objective for optimization.

## 2.2 LIKELIHOOD WITH DEPENDENCIES

Assuming the data points are identically distributed, but **not independently** distributed, the joint density does not factorize anymore. A model trained on non-independent data but under independence assumptions will hence yield biased results for both density estimation and data generation.

We can derive the non-independent setting as follows. Let  $T : \mathbb{R}^{n \times p} \rightarrow \mathbb{R}^{n \times p}$  be the normalizing flow applied on all data points together, i.e.,

$$U = T^{-1}(X) = T^{-1}(x_1, \dots, x_n) = \begin{pmatrix} t^{-1}(x_1)^\top \\ \vdots \\ t^{-1}(x_n)^\top \end{pmatrix}.$$

$X, U \in \mathbb{R}^{n \times p}$  are now matrix-variate random variables. We can still apply the change of variable formula, but on the  $n \times p \rightarrow n \times p$  transformation  $T$ , instead of the  $p \rightarrow p$  transformation  $t$ :

$$\log(p_X(X)) = \log(p_U(U)) - \log(|\det J_T(U)|).$$

If  $T$  is understood on  $np$  instead of  $n \times p$  space, it becomes clear that the Jacobian  $J_T$  is a block-diagonal matrix,

$$J_T(U) = \begin{pmatrix} J_t(u_1) & 0 & \dots & 0 \\ 0 & J_t(u_2) & & \\ \vdots & & & \\ 0 & \dots & & J_t(u_n) \end{pmatrix},$$

for which the determinant is readily available:  $\det J_T(U) = \prod_{i=1}^n J_t(u_i)$ . In other words, the log-abs-det term in the normalizing flow objective remains unchanged even under arbitrary dependence structure.

The density  $p_U(U)$ , however, is challenging and generally not tractable, and we will consider different assumptions on the joint distribution of  $U$ .

In the most general case, we could assume that each  $u_i$  is marginally distributed as a  $\mathcal{U}_{[0,1]^p}$  variable, with arbitrary dependence structure across observations. This is a direct extension of standard copulas to matrix-variate variables. As learning general copulas is extremely challenging even in relatively low dimensional settings (Jaworski et al., 2010), we focus in this work only on the equivalent of a Gaussian copula:

**Assumption 2.1.** We assume that the dependency within  $U$  can be modeled by a matrix normal distribution  $\mathcal{MN}$  with independent columns (within observations), but correlated rows (between observations):

$$U \sim \mathcal{MN}_{n,p}(0, C, I_p) \triangleq \mathcal{N}_{np}(0, I_p \otimes C).$$

Here,  $\otimes$  denotes the Kronecker product.

We can model the columns of  $U$  with a 0-mean vector and  $I_p$ -covariance, as the normalizing flow  $t$  is usually chosen to be expressive enough to transform a  $\mathcal{N}_p(0, I_p)$  into the desired data distribution. We note that this assumption means that we cannot model all forms of latent dependencies so it constitutes a trade-off between expressivity and tractability.

Now we can state the full likelihood in the non-i.i.d. setting:

$$\log(p_X(X)) = - \sum_{i=1}^n \log(|\det J_t(u_i)|) - \frac{np}{2} \log(2\pi) - \frac{p}{2} \log(\det(C)) - \frac{1}{2} \text{tr}(U^\top C^{-1}U). \quad (1)$$

## 2.3 SPECIFIC COVARIANCE STRUCTURES

We investigate different assumptions on the covariance structure in the latent dependency model. The most general case is a fully unspecified covariance matrix, e.g. parametrized as the lower-triangular Cholesky decomposition of its inverse,  $C = L^{-1}L^{-\top}$  with  $n(n+1)/2$  parameters. In

this case, the determinant can be efficiently computed, as  $\det(C) = \det(L^{-1}L^{-\top}) = \det(L^{-1})^2 = \prod_{i=1}^n (L^{-1})_{i,i}^2$ . Matrix products with  $C^{-1}$  can also be evaluated reasonably fast. However, this parametrization requires optimizing  $O(n^2)$  additional parameters, which is unlikely to yield useful estimates and may be prone to overfitting.

Instead, we consider two different assumptions on  $C$  that are very common in practice and give a reasonable trade-off between expressivity and statistical efficiency.

### 2.3.1 KNOWN AND FIXED COVARIANCE MATRIX

In many settings, side information can yield relationship information, given in the form of a fixed relationship matrix  $G$ . The covariance matrix then becomes  $C = \lambda I_n + (1-\lambda)G$  with only parameter  $\lambda \in [0, 1]$  to be determined.

This setting is commonly assumed for confounding correction in genetic association studies, where  $G$  is a genetic relationship matrix (where the entries are pairwise genetic relationships computed from allele frequencies (Lippert et al., 2011)) or based on pedigree information (e.g., a parent-child pair receives a relationship coefficient of 0.5 and a grandparent-grandchild pair of 0.25 (Visscher et al., 2012)). Similarly, for time-related data, we can define relationship via, e.g., a negative exponential function:  $C_{i,j} = \exp(-\gamma(t_i - t_j)^2)$ , where the hyperparameter  $\gamma > 0$  is a time-decay factor and  $t_i$  and  $t_j$  are the measurement time points of observations  $i$  and  $j$ , respectively.

More generally,  $G$  itself can again be a mixture of multiple relationships  $G = \sum_{r=1}^R G_r$ , where  $G_r$  denote multiple sources of relatedness. In this work, we consider  $G$  to be fully specified and only estimate  $\lambda$ .

If the sample size is moderate (say, below 50k), an efficient approach to optimizing  $\lambda$  (Lippert et al., 2011) consists of first computing the spectral decomposition of  $G = Q\Lambda Q^\top$  (with diagonal  $\Lambda$  and orthogonal  $Q$ ) and then noticing that

$$\lambda I_n + (1 - \lambda)G = Q(\lambda I_n + (1 - \lambda)\Lambda)Q^\top.$$

Then, the log-determinant and the trace are

$$\begin{aligned} \log(\det(C)) &= \sum_{i=1}^n \log(\lambda + (1 - \lambda)\Lambda_{i,i}), \text{ and} \\ \text{tr}(U^\top C^{-1}U) &= \text{tr}((Q^\top U)^\top (\lambda I_n + (1 - \lambda)\Lambda)^{-1} Q^\top U). \end{aligned}$$

The rotation matrix  $Q$  makes mini-batch estimation of the trace term inefficient, as  $Q$  will either mix  $U$  across batches or requires a full re-evaluation of  $Q(\lambda I_n + (1 - \lambda)\Lambda)^{-1}Q^\top$  after each update to  $\lambda$ , i.e., in every mini-batch. Instead, we optimize the parameters of the normalizing flow and  $\lambda$  in an alternating two-step procedure, see Section 2.4.2. Note that the main additional cost of this procedure, the spectral decomposition of  $G$ , is independent of  $\lambda$  and only needs to be performed once for a given relationship matrix  $G$ .

For larger sample sizes, there still exist practical algorithms for estimating the variance component (Loh et al., 2015). In practice,  $G$  is also often sparse or can be approximated sparsely (e.g., by setting all elements with absolute value below a fixed threshold to 0). This can greatly accelerate parameter estimation and is usually accurate enough in practice (Jiang et al., 2019). More generally, different matrix structures may allow for additional speed-ups, but we defer this investigation to future work.

### 2.3.2 BLOCK-DIAGONAL, EQUICORRELATED COVARIANCE STRUCTURE

In the next setting, we consider a *block-diagonal* covariance matrix

$$C = \begin{pmatrix} C_1 & 0 & \dots & 0 \\ 0 & C_2 & & \\ \dots & & & \\ 0 & \dots & & C_N \end{pmatrix}$$

where each block  $C_i \in \mathbb{R}^{n_i \times n_i}$  is an *equicorrelated correlation matrix*:

$$C_i = \begin{pmatrix} 1 & \rho_i & \dots & \rho_i \\ \rho_i & 1 & & \\ \dots & & & \\ \rho_i & \dots & & 1 \end{pmatrix}.$$

with  $\rho_i \in (0, 1)$  (we ignore the case of potentially anti-correlated blocks). In other words, there is no dependence between blocks, and there is a constant dependence within blocks. We assume that the *block structure* is known ahead and we only need to find the parameters  $\rho_i$ . For each block there is either no ( $n_i = 1$ ) or only one ( $n_i > 1$ ) parameter to be learned.

The assumption of equicorrelated blocks is reasonable in settings with *repeat measurements* of identical objects or individuals. E.g., in a facial image data set, certain individuals may have multiple images. This setting is similar to the setting of high-cardinality categorical features in prediction models (Simchoni & Rosset, 2021).

The determinant of  $C$  is the product of the determinants of the individual blocks  $C_i$ , and the determinant of each  $C_i$  can be computed, following Tong (2012), Prop. 5.2.1, as:

$$\det(C_i) = (1 + (n_i - 1)\rho_i)(1 - \rho_i)^{n_i - 1}.$$

The inverse of  $C_i$  has a similarly efficient representation (Prop. 5.2.3 in Tong (2012)):

$$(C_i^{-1})_{j,k} = \begin{cases} \frac{1+(n_i-2)\rho_i}{(1-\rho_i)(1+(n_i-1)\rho_i)} & \text{if } j = k \\ \frac{-\rho_i}{(1-\rho_i)(1+(n_i-1)\rho_i)} & \text{otherwise.} \end{cases}$$

## 2.4 OPTIMIZATION

### 2.4.1 MINI-BATCH ESTIMATION

The full likelihood in equation 1 can be computed explicitly but does not lend itself easily to stochastic optimization with mini-batches (the default optimization procedure in deep learning). Note that the log-abs-det term decomposes nicely into independent observations, the next two terms are independent of the observations, and only the trace term is problematic for mini-batch estimation. We next propose an unbiased stochastic estimator of the trace term.

**Proposition 2.2.** *Given a mini-batch of size  $b \geq 2$  and  $\xi \in \{0, 1\}^n$  a variable indicating batch inclusion (i.e.,  $x_i$  is in batch iff  $\xi_i = 1$ ;  $\sum_{i=1}^n \xi_i = b$ ) and  $A := C^{-1}$ , the stochastic trace estimator*

$$\bar{tr}_\xi = \frac{n}{b} \sum_{i=1}^n \xi_i A_{i,i} u_i^\top u_i + 2 \frac{n(n-1)}{b(b-1)} \sum_{i < j} \xi_i \xi_j A_{i,j} u_i^\top u_j$$

is unbiased, i.e.,  $\mathbb{E}_\xi[\bar{tr}_\xi] = \text{tr}(U^\top AU)$ .

The proof can be found in Appendix A.1.

The trace estimator  $\bar{tr}_\xi$  only depends on observations  $u_i = t^{-1}(x_i)$  within the batch and can be efficiently computed, assuming  $A = C^{-1}$  can be efficiently evaluated, which is the case for the parametrizations discussed in Section 2.3.

The resulting (rescaled) mini-batch likelihood objective for mini-batch  $\xi$  is:

$$\begin{aligned} & - \sum_{i:\xi_i=1} \log(|\det J_t(u_i)|) - \frac{bp}{2} \log(2\pi) - \frac{bp}{n2} \log(\det(C)) \\ & - \frac{1}{2} \sum_{i:\xi_i=1}^n A_{i,i} u_i^\top u_i - \frac{n-1}{b-1} \sum_{i < j:\xi_i=\xi_j=1} A_{i,j} u_i^\top u_j. \end{aligned} \quad (2)$$

### 2.4.2 TRAINING SCHEDULES

From here on, we distinguish between the true parameters  $\lambda$  and  $\rho_i$ , and the parameters estimated by our model,  $\hat{\lambda}$ ,  $\hat{\rho}_i$ .

**Known & Fixed Covariance** Joint optimization between  $\hat{\lambda}$  and the parameters of the flow is possible, but would require in each step a full re-evaluation  $\text{tr}(U^\top C^{-1}U)$  across the full data set, instead of just the current mini-batch. This makes this training scheme infeasible. Instead, we propose two different methods to optimize both the flow parameters and variance component  $\hat{\lambda}$ .

First, we can use a simple **grid search** over different possible values for  $\hat{\lambda}$  and choose the best according to performance on a validation set.

Second, we can use an **alternating descent** approach. In this case, we alternate between optimizing only the parameters of the flow model for a number of epochs (with a version of mini-batch stochastic gradient descent) and only optimizing  $\hat{\lambda}$  for a number of epochs (with gradient descent). At the beginning of every flow-parameter training stage, we compute the current  $A = C^{-1}$  for the given  $\hat{\lambda}$  and can then compute all mini-batch likelihood estimates given the formula in Equation 2 without the need for recomputation. At the beginning of every  $\hat{\lambda}$  training stage, we only once compute the rotated noise variables  $Q^\top U$  for the full data set and can then optimize the derivative of the full objective with respect to  $\hat{\lambda}$  very efficiently. The trace can be computed as  $\text{tr}((Q^\top U)^\top (\hat{\lambda}I_n + (1 - \hat{\lambda})\Lambda)^{-1} Q^\top U)$  or as  $\text{tr}(Q^\top U (Q^\top U)^\top (\hat{\lambda}I_n + (1 - \hat{\lambda})\Lambda)^{-1})$  due to the cyclical trace property, but in our experiments we found that this was not a bottleneck computation. To yield values in the interval  $[0, 1]$ , we chose to parametrize  $\hat{\lambda}$  as the output of a sigmoid function  $\hat{\lambda} = \sigma(\hat{\lambda}_{raw})$ , where  $\hat{\lambda}_{raw} \in \mathbb{R}$  is the raw optimization parameter. We tried different sigmoidal parametrizations, but those had little effect on the outcome.

**Equicorrelated Blocks** In the case of equicorrelated blocks, we also propose two different training schemes.

First, we can again use a simple **grid search** over a single joint parameter  $\hat{\rho} = \hat{\rho}_1 = \dots = \hat{\rho}_N$ . Alternatively, if there are only very few blocks, a grid search for all  $\hat{\rho}_i$  is possible, although the exploration space grows exponentially with the number of blocks  $N$ .

Second, due to the simple computations of  $\det(C)$  and  $C^{-1}$  in this case, we can also perform a **joint** optimization over the flow parameters and all  $\hat{\rho}_i$ . We again parametrize  $\hat{\rho}_i$ s with raw parameters pushed through a sigmoid function as for  $\hat{\lambda}$ .

### 3 EXPERIMENTAL EVALUATION

We validate on both synthetic and real-world data that our novel training scheme can help alleviate sampling biases when training normalizing flows. On real-world data with non-independent data, the ground-truth dependency structure is usually not known, making the evaluation inherently challenging. Therefore, we first investigate simulated settings where we can explicitly control the dependencies. All experiments were implemented in PyTorch (Paszke et al., 2019) and PyTorch Lightning, using the normalizing flow implementations provided by Nielsen et al. (2020). In all settings, we use the Adamax optimizer (Kingma & Ba, 2015) and reduce the learning rate with an exponential decay. Weight decay (chosen as described below) is always only applied to the weights of the normalizing flows, not on the dependency parameters  $\hat{\lambda}$  and  $\hat{\rho}_i$ . Our evaluation metric in all settings is the negative log-likelihood (NLL) on a holdout test set. For the imaging experiment, we also report bits per dimension (bpd), a linear transformation of the NLL.

#### 3.1 SYNTHETIC DATA EXPERIMENTS

##### 3.1.1 EQUICORRELATED DATA

In the first setting, we simulate a draw with repeat measurements, inducing an equicorrelated dependency structure as described in Section 2.3.2. Namely, we sample block-sizes from a Pareto II distribution with shape parameter  $\alpha = 0.5$  and minimum value 1, rounded to integer values. We clip block-sizes to a maximum of 1,000 and draw new blocks until all blocks together sum to  $n = 10,000$  samples. For each block, we draw one  $\rho_i \sim \text{Unif}_{[0.5, 0.99]}$  and define the full covariance matrix as in Section 2.3.2. Using this covariance matrix, we sample non-independently from a bivariate standard normal distribution. We non-linearly transform these data into complex shapes

Table 1: Results in terms of the test-data negative log-likelihoods for synthetic data with equicorrelated blocks (top) and fixed covariance (bottom), averaged over 10 random seeds (lower = better). Significantly better results are in bold (one-sided paired t-test,  $\alpha = 0.05$ ). Baseline is the same model without taking dependencies into consideration.

	Algorithm	Abs	Crescent	CrescentCubed	Sign	SineWave
Equicorrelated Blocks	Baseline	1.513	2.021	3.010	1.519	2.070
	Grid Search	<b>1.379</b>	<b>1.885</b>	<b>2.938</b>	<b>1.420</b>	<b>1.983</b>
	Joint	1.475	2.005	3.067	1.501	2.087
Fixed Covariance	Baseline	1.590	2.144	3.262	1.818	2.353
	Grid Search	<b>1.376</b>	<b>1.866</b>	<b>2.944</b>	<b>1.443</b>	<b>2.040</b>
	Alternating	<b>1.361</b>	<b>1.869</b>	<b>2.915</b>	<b>1.430</b>	<b>2.064</b>

(Abs, Crescent, CrescentCubed, Sign, and SineWave) provided by Durkan et al. (2019), for a more challenging density estimation task. We repeat all experiments 10 times with different random seeds.

An example for the Abs data set can be seen in Figure 1. As a base flow model, we choose rational quadratic spline flows (Durkan et al., 2019), which are state-of-the-art for these challenging data sets. For modelling the equicorrelated blocks, we choose both a grid search over fixed parameters  $\hat{\rho} \in \{0.01, 0.025, 0.05, 0.1, 0.175, 0.25, 0.375, 0.5, 0.6, 0.67, 0.75, 0.9\}$  and joint gradient-based optimization of  $\hat{\rho}_i$  and the flow parameters, with starting values for  $\hat{\rho}_i \in \{0.01, 0.1, 0.25, 0.5\}$ . We train all models for 100 epochs, perform a small hyperparameter sweep over learning rate (in  $\{0.001, 0.003, 0.01, 0.03\}$ ) and weight decay (in  $\{0.001, 0.01, 0.1\}$ ), and choose the best model for each setting based on early stopping and validation set performance (which is sampled *without* dependencies).

Table 1 (top part) shows the result. Surprisingly, while the grid search clearly outperforms the baseline model, the joint optimization does not improve upon the model. We investigated a number of adaptations on the learning schedule for the joint optimization, but found no significant improvements. For the Crescent data set we also computed the distance of learned  $\hat{\rho}_i$ s to true  $\rho_i$ s for the best models (each block is counted only once, independent of size). The baseline model had an average MSE of 0.57 (MAE: 0.74), while the grid search had MSEs of only 0.023 (MAE: 0.13) and 0.08 (MAE: 0.25), respectively.

In an additional experiment, this time only on the Crescent data set, we investigate how sensitive our model is to the strength of dependencies. In the data creation, we only change the sampling of true dependency parameters  $\rho_i$  from a  $\text{Unif}_I$  distribution, with interval  $I \in \{[0, 0.2], [0.2, 0.4], [0.4, 0.6], [0.6, 0.8], [0.8, 1.0]\}$ . We use a grid search, select hyperparameters for all models as before, and repeat all experiments with ten random seeds. The results are shown in Figure 2. We find that at each of the five data set settings, a one-sided paired t-test shows that the normalizing flow incorporating dependencies outperforms the baseline (significance level  $\alpha = 0.05$ ). As expected, for small dependencies in the true data, both models perform similarly. Interestingly, our method is extremely robust and barely decreases in performance up until the highest range of sampling distortions.

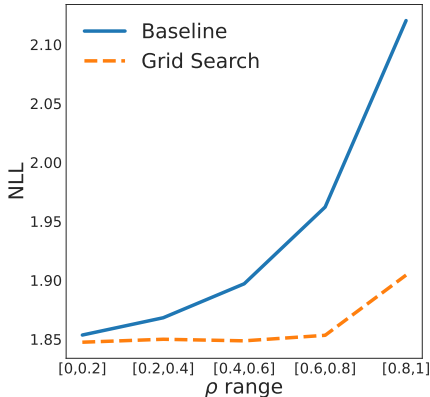


Figure 2: Performance of baseline model versus model adjusted for dependencies, for different strengths of dependencies ( $\rho$ ).

Table 2: Results on real-world data, negative log-likelihoods on test data set, averaged over 10 random seeds for UKB & Stock Pair data (lower = better). P-values for one-sided paired t-test against baseline in parentheses. Baseline is same model without taking dependencies into consideration.

Algorithm	UKB Biomarkers	Stock Pairs	ADNI (bpd)
Baseline	24.50	-5.69	7836.5 (2.760)
Grid Search	24.27 ( $p = 0.002$ )	-5.72 ( $p = 0.002$ )	7725.8 (2.721)
Joint		-5.71 ( $p = 0.003$ )	7715.8 (2.718)
Alternating	24.04 ( $p = 0.00003$ )		

### 3.1.2 KNOWN COVARIANCE

In this setting, we simulate the setting of a known covariance matrix between different samples (this time  $n = 5,000$ ) but with unknown variance component  $\lambda$ . We first draw a lower-triangular matrix  $L$ , with diagonals all set to 1 and all elements below the diagonal drawn independently from  $\text{Unif}_{[0.5, 0.99]}$ . We use  $G = \text{norm}(LL^T)$  as our covariance structure, where  $\text{norm}$  normalizes the covariance matrix to a correlation matrix (with all-1s on the diagonal). We then use the covariance structure  $\lambda I + (1 - \lambda)G$  as in the equicorrelated case to generate correlated bivariate standard normal samples that again get non-linearly transformed. We fix  $\lambda = 0.5$  in all experiments, and experiments are again repeated 10 times.

For the grid search, we choose  $\hat{\lambda} \in \{0.99, 0.975, 0.95, 0.9, 0.825, 0.75, 0.625, 0.5, 0.4, 0.33, 0.25, 0.1\}$  (note that  $\lambda$  corresponds to  $1 - \rho$ ) and for the alternating optimization scheme, we initialize  $\hat{\lambda}$  from  $\{0.99, 0.9, 0.75, 0.5\}$ . We train for 100 epochs in the baseline and in grid search; for the alternating optimization, we train for 5 stages of 25 epochs for the flow optimization, with 4 stages of 100 gradient descent updates of  $\hat{\lambda}$  inbetween. Remaining parameters are chosen as in the equicorrelated simulations.

In Table 1 (bottom part) we compare the results. Both the simple grid search and the alternating descent approach perform considerably better than the naive baseline algorithm that ignores the dependencies in the data.

## 3.2 REAL-WORLD DATA

Next we investigate three real-world applications. All results are summarized in Table 2.

### 3.2.1 UKB BIOMARKERS

The UK Biobank (UKB, (Bycroft et al., 2018)) provides rich phenotyping and genotyping for a large cross-section of the UK population. We investigate a number of blood biomarkers, whose distribution starkly deviates from standard parametric distributions such as a normal distribution. Usually, the data needs to be quantile-transformed to match a normal distribution (Monti et al., 2022), which, however, can decrease power of many statistical methods (McCaw et al., 2020). These biomarkers are well-known to be highly heritable and subject to population stratification, a type of confounding due to joint ancestry of unrelated individuals (Sinnott-Armstrong et al., 2021).

In this experiment, we build a non-parametric density model that can incorporate the distorting genetic correlation between individuals. We select the 3,223 individuals for whom all 30 biomarkers are available. Relatedness between two individuals is computed as the correlation coefficients between the individuals' first 40 (unnormalized) genetic principal components (computed from SNP microarray chip data provided by the UKB resource). This way of measurement of genetic relatedness between individuals is very common in genetic association studies and has been shown to reliably correct for population stratification (Price et al., 2006).

Due to the relatively small data set size, we re-run the same experiment 10 times with different random splits between train, validation, and test set and also different network initializations. The results indicate that incorporating the dependencies can significantly improve model fit, both using a grid search and using the alternating optimization scheme.

---

### 3.2.2 STOCK DATA PAIRS

A range of different stock trading and risk management strategies require accurate modeling of the behavior of different stocks (Kole et al., 2007). We focus on modeling the daily returns for two pairs of correlated stocks, which is used, e.g., in pair trading strategies (Stander et al., 2013). Namely, we use the pairs `AAPL-MSFT` (Apple and Microsoft) and `MA-V` (Mastercard and Visa), each starting from initial public offering (IPO) of the later of the pair, until late 2017, using publicly available data at close time. A single data point is the 2-dimensional logarithmic return of one of the two pairs of stocks. We split data into train (70%), validation (15%), and test (15%) data temporally (non-randomly) to counteract data leakage. Since Apple and Microsoft had their respective IPOs in the 1980s and Visa and Mastercard theirs in the 2000s, the `AAPL-MSFT` pair is overrepresented in the training data, while both pairs are equally represented in the validation and test data. We use the equicorrelated dependency model with two blocks, one for `AAPL-MSFT` and one for `MA-V`. The distribution fit for the equicorrelated model is slightly improved using the data dependencies, but again showing that a joint optimization appears to be inferior to a simple grid search.

### 3.2.3 ADNI BRAIN IMAGING

Finally, we apply our method to brain imaging data from the Alzheimer’s Disease Neuroimaging Initiative (ADNI, (Jack Jr et al., 2008)). Prior work on similar data has shown that causal effects can be modeled in generative image models using explicit confounding factors such as age and sex (Pawlowski et al., 2020). Here we show that we can also model the i.i.d.-violations using our proposed method. The data are T1-weighted MRI, preprocessed and standardized with a brain extraction, linear alignment, non-linear alignment, and debiasing pipeline. We select the axial-view centered slices and resize them to  $64 \times 64$  grayscale images. As ADNI is a longitudinal study of Alzheimer’s Disease (AD) progression, many of the individuals in the study are imaged multiple times. The data set comprises 1,820 individuals with each individual having between 1 and 35 images (mean: 7.03, median: 6) and a total of 12,799 images. We model these repeat measurements with the equicorrelated model and use a Glow-type image normalizing flow (Kingma & Dhariwal, 2018) as our base architecture with two scales and twelve steps per scale. We trained all models with a batch-size of 64 and learning rate and weight decay of 0.001 for 200 epochs on a single A100 GPU. Due to compute constraints, no further hyperparameter exploration was performed. Grid search and initialization for joint optimization was  $\hat{\rho}_i \in \{0.01, 0.025, 0.05, 0.075, 0.1, 0.15\}$ , and the  $\hat{\rho}_i$  chosen by the best final model with joint optimization ranged between 0.066 and 0.081.

The results show that incorporating the dependencies can improve the density estimation on the holdout test data set considerably, with a slight edge for the joint optimization. Sample images from the train data and the flow models are shown in Figure 3 in the Appendix.

## 4 CONCLUSION

We have shown that through a simple adaptation in the likelihood loss of normalizing flows, we can integrate flexible data dependencies into the training objective, which can also be trained with mini-batch stochastic gradient descent. Experimental evaluation of synthetic and real-world data showed that our method can significantly improve the fit of probabilistic models. In future work, we’re especially interested how our method can be extended to other generative models such as VAEs and if it can be combined with other debiasing methods such as causal DAGs as done by Pawlowski et al. (2020).

Our method is not without limitations. The mini-batch loss in Equation 2 is unbiased, but has a high variance due to the overweighting of the off-diagonal terms. This can lead to unstable gradient estimates, especially in the early stages of training. In addition, joint optimization of  $\hat{\rho}_i$ s with the flow parameters counterintuitively only sometimes leads to better results. We believe further improvements to the optimization schemes might alleviate these issues.

We also note that, if the goal is density estimation or generative modeling, incorporating dependencies into the normalizing flow objective is not necessary in *all* cases with dependent data. For example, in the case of equicorrelated repeat measurements with *identical block-sizes*, no improvements can be expected. This is because no region of the sampling space is overrepresented relative to the other regions. Only when some blocks are larger than others (or with more general, unbalanced

---

covariance matrices), adjustment for dependencies makes sense. However, if we are interested in *full likelihood evaluation* over the whole data set instead of just density estimation in individual data points, the results will differ.

## REFERENCES

- Sean Augenstein, H. Brendan McMahan, Daniel Ramage, Swaroop Ramaswamy, Peter Kairouz, Mingqing Chen, Rajiv Mathews, and Blaise Aguerre y Arcas. Generative models for effective ml on private, decentralized datasets. In *International Conference on Learning Representations*, 2020. URL <https://openreview.net/forum?id=SJgARA4FPH>.
- Clare Bycroft, Colin Freeman, Desislava Petkova, Gavin Band, Lloyd T Elliott, Kevin Sharp, Allan Motyer, Damjan Vukcevic, Olivier Delaneau, Jared O’Connell, et al. The uk biobank resource with deep phenotyping and genomic data. *Nature*, 562(7726):203–209, 2018.
- Lon R Cardon and Lyle J Palmer. Population stratification and spurious allelic association. *The Lancet*, 361(9357):598–604, 2003.
- Laurent Dinh, Jascha Sohl-Dickstein, and Samy Bengio. Density estimation using real NVP. In *International Conference on Learning Representations*, 2017. URL <https://openreview.net/forum?id=HkpbhH9lx>.
- Conor Durkan, Artur Bekasov, Iain Murray, and George Papamakarios. Neural spline flows. *Advances in neural information processing systems*, 32, 2019.
- Clifford R Jack Jr, Matt A Bernstein, Nick C Fox, Paul Thompson, Gene Alexander, Danielle Harvey, Bret Borowski, Paula J Britson, Jennifer L. Whitwell, Chadwick Ward, et al. The alzheimer’s disease neuroimaging initiative (adni): Mri methods. *Journal of Magnetic Resonance Imaging: An Official Journal of the International Society for Magnetic Resonance in Medicine*, 27(4):685–691, 2008.
- Piotr Jaworski, Fabrizio Durante, Wolfgang Karl Hardle, and Tomasz Rychlik. *Copula theory and its applications*, volume 198. Springer, 2010.
- Jiming Jiang and Thuan Nguyen. *Linear and generalized linear mixed models and their applications*, volume 1. Springer, 2007.
- Longda Jiang, Zhili Zheng, Ting Qi, Kathryn E Kemper, Naomi R Wray, Peter M Visscher, and Jian Yang. A resource-efficient tool for mixed model association analysis of large-scale data. *Nature genetics*, 51(12):1749–1755, 2019.
- Diederik P. Kingma and Jimmy Ba. Adam: A method for stochastic optimization. *CoRR*, abs/1412.6980, 2015.
- Durk P Kingma and Prafulla Dhariwal. Glow: Generative flow with invertible 1x1 convolutions. *Advances in neural information processing systems*, 31, 2018.
- Erik Kole, Kees Koedijk, and Marno Verbeek. Selecting copulas for risk management. *Journal of Banking & Finance*, 31(8):2405–2423, 2007.
- Christoph Lippert, Jennifer Listgarten, Ying Liu, Carl M Kadie, Robert I Davidson, and David Heckerman. Fast linear mixed models for genome-wide association studies. *Nature methods*, 8(10):833–835, 2011.
- Po-Ru Loh, George Tucker, Brendan K Bulik-Sullivan, Bjarni J Vilhjalmsson, Hilary K Finucane, Rany M Salem, Daniel I Chasman, Paul M Ridker, Benjamin M Neale, Bonnie Berger, et al. Efficient bayesian mixed-model analysis increases association power in large cohorts. *Nature genetics*, 47(3):284–290, 2015.
- Zachary R McCaw, Jacqueline M Lane, Richa Saxena, Susan Redline, and Xihong Lin. Operating characteristics of the rank-based inverse normal transformation for quantitative trait analysis in genome-wide association studies. *Biometrics*, 76(4):1262–1272, 2020.

- 
- Remo Monti, Pia Rautenstrauch, Mahsa Ghanbari, Alva Rani James, Matthias Kirchler, Uwe Ohler, Stefan Konigorski, and Christoph Lippert. Identifying interpretable gene-biomarker associations with functionally informed kernel-based tests in 190,000 exomes. *Nature communications*, 13(1): 1–16, 2022.
- Didrik Nielsen, Priyank Jaini, Emiel Hoogeboom, Ole Winther, and Max Welling. Survae flows: Surjections to bridge the gap between vaes and flows. *Advances in Neural Information Processing Systems*, 33:12685–12696, 2020.
- George Papamakarios, Eric T Nalisnick, Danilo Jimenez Rezende, Shakir Mohamed, and Balaji Lakshminarayanan. Normalizing flows for probabilistic modeling and inference. *J. Mach. Learn. Res.*, 22(57):1–64, 2021.
- Adam Paszke, Sam Gross, Francisco Massa, Adam Lerer, James Bradbury, Gregory Chanan, Trevor Killeen, Zeming Lin, Natalia Gimelshein, Luca Antiga, Alban Desmaison, Andreas Kopf, Edward Yang, Zachary DeVito, Martin Raison, Alykhan Tejani, Sasank Chilamkurthy, Benoit Steiner, Lu Fang, Junjie Bai, and Soumith Chintala. Pytorch: An imperative style, high-performance deep learning library. In H. Wallach, H. Larochelle, A. Beygelzimer, F. d'Alché-Buc, E. Fox, and R. Garnett (eds.), *Advances in Neural Information Processing Systems 32*, pp. 8024–8035. Curran Associates, Inc., 2019. URL <http://papers.neurips.cc/paper/9015-pytorch-an-imperative-style-high-performance-deep-learning-library.pdf>.
- Nick Pawlowski, Daniel Coelho de Castro, and Ben Glocker. Deep structural causal models for tractable counterfactual inference. *Advances in Neural Information Processing Systems*, 33:857–869, 2020.
- Alkes L Price, Nick J Patterson, Robert M Plenge, Michael E Weinblatt, Nancy A Shadick, and David Reich. Principal components analysis corrects for stratification in genome-wide association studies. *Nature genetics*, 38(8):904–909, 2006.
- Mohammad Rasouli, Tao Sun, and Ram Rajagopal. Fedgan: Federated generative adversarial networks for distributed data. *arXiv preprint arXiv:2006.07228*, 2020.
- Danilo Rezende and Shakir Mohamed. Variational inference with normalizing flows. In *International conference on machine learning*, pp. 1530–1538. PMLR, 2015.
- Felix Salmon. Recipe for disaster: the formula that killed wall street. *Wired Magazine*, 17(3):17–03, 2009.
- Giora Simchoni and Saharon Rosset. Using random effects to account for high-cardinality categorical features and repeated measures in deep neural networks. *Advances in Neural Information Processing Systems*, 34, 2021.
- Nasa Sinnott-Armstrong, Yosuke Tanigawa, David Amar, Nina Mars, Christian Benner, Matthew Aguirre, Guhan Ram Venkataraman, Michael Wainberg, Hanna M Ollila, Tuomo Kiiskinen, et al. Genetics of 35 blood and urine biomarkers in the uk biobank. *Nature genetics*, 53(2):185–194, 2021.
- Yolanda Stander, Daniël Marais, and Ilse Botha. Trading strategies with copulas. *Journal of Economic and Financial Sciences*, 6(1):83–107, 2013.
- Yung Liang Tong. *The multivariate normal distribution*. Springer Science & Business Media, 2012.
- M-N Tran, Nghia Nguyen, David Nott, and Robert Kohn. Bayesian deep net glm and glmm. *Journal of Computational and Graphical Statistics*, 29(1):97–113, 2020.
- Peter M Visscher, Matthew A Brown, Mark I McCarthy, and Jian Yang. Five years of gwas discovery. *The American Journal of Human Genetics*, 90(1):7–24, 2012.
- Yunyang Xiong, Hyunwoo J Kim, and Vikas Singh. Mixed effects neural networks (menets) with applications to gaze estimation. In *Proceedings of the IEEE/CVF Conference on Computer Vision and Pattern Recognition*, pp. 7743–7752, 2019.

---

## ACKNOWLEDGMENTS

The authors would like to thank Philipp Liznerski and Alexander Rakowski for helpful discussions, and Alexander Rakowski for providing the MRI processing pipeline used on ADNI data. This work was supported by the German Ministry of Research and Education (Bundesministerium für Bildung und Forschung—BMBF) in the SyReal project (project number 01IS21069A), the DFG awards KL 2698/2-1, KL 2698/5-1, KL 2698/6-1, and KL 2698/7-1, and the BMBF awards 01—S18051A, 03—B0770E, and 01—S21010C. MKloft acknowledges support by the Carl-Zeiss Foundation. This research has been conducted using the UK Biobank Resource. Data collection and sharing for this project was funded by the Alzheimer’s Disease Neuroimaging Initiative (ADNI) (National Institutes of Health Grant U01 AG024904) and DOD ADNI (Department of Defense award number W81XWH-12-2-0012). ADNI is funded by the National Institute on Aging, the National Institute of Biomedical Imaging and Bioengineering, and through generous contributions from the following: AbbVie, Alzheimer’s Association; Alzheimer’s Drug Discovery Foundation; Araclon Biotech; BioClinica, Inc.; Biogen; Bristol-Myers Squibb Company; CereSpir, Inc.; Cogstate; Eisai Inc.; Elan Pharmaceuticals, Inc.; Eli Lilly and Company; EuroImmun; F. Hoffmann-La Roche Ltd and its affiliated company Genentech, Inc.; Fujirebio; GE Healthcare; IXICO Ltd.; Janssen Alzheimer Immunotherapy Research & Development, LLC.; Johnson & Johnson Pharmaceutical Research & Development LLC.; Lumosity; Lundbeck; Merck & Co., Inc.; Meso Scale Diagnostics, LLC.; NeuroRx Research; Neurotrack Technologies; Novartis Pharmaceuticals Corporation; Pfizer Inc.; Piramal Imaging; Servier; Takeda Pharmaceutical Company; and Transition Therapeutics. The Canadian Institutes of Health Research is providing funds to support ADNI clinical sites in Canada. Private sector contributions are facilitated by the Foundation for the National Institutes of Health ([www.fnih.org](http://www.fnih.org)). The grantee organization is the Northern California Institute for Research and Education, and the study is coordinated by the Alzheimer’s Therapeutic Research Institute at the University of Southern California. ADNI data are disseminated by the Laboratory for Neuro Imaging at the University of Southern California.

## A APPENDIX

### A.1 PROOF OF PROPOSITION 2.2

We have

$$\mathbb{E}_\xi[\bar{tr}_\xi] = \frac{n}{b} \sum_{i=1}^n \mathbb{E}_\xi[\xi_i] A_{i,i} u_i^\top u_i + 2 \frac{n(n-1)}{b(b-1)} \sum_{i < j} \mathbb{E}_\xi[\xi_i \xi_j] A_{i,j} u_i^\top u_j.$$

For the first term, we know that  $\mathbb{E}_\xi[\xi_i] = b/n$ , so

$$\frac{n}{b} \sum_{i=1}^n \mathbb{E}_\xi[\xi_i] A_{i,i} u_i^\top u_i = \sum_{i=1}^n A_{i,i} u_i^\top u_i.$$

For the second term, we first note that

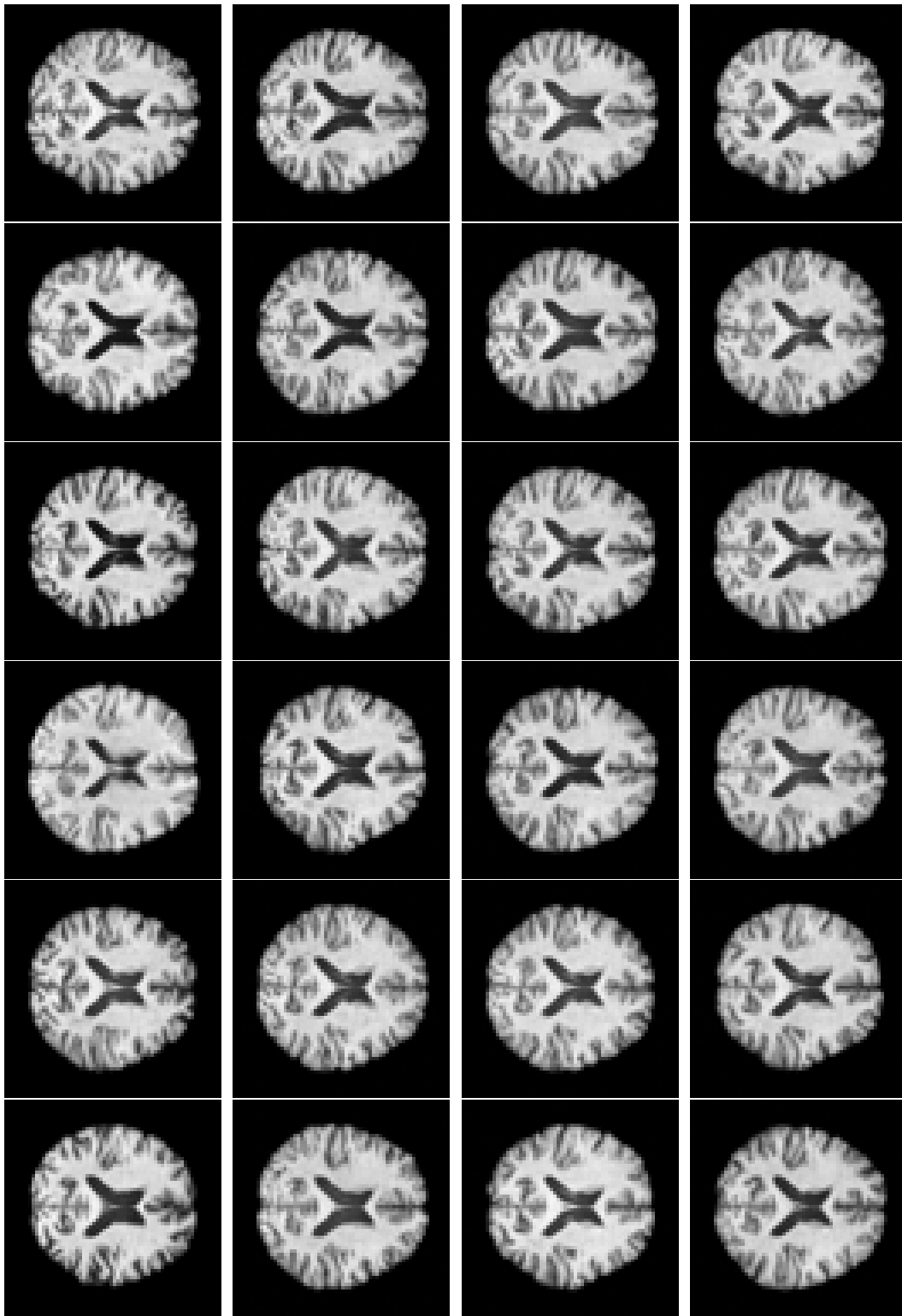
$$\mathbb{E}_\xi[\xi_i \xi_j] = \mathbb{E}_\xi[\xi_i E_\xi[\xi_j | \xi_i]] = \frac{b}{n} \mathbb{E}_\xi[\xi_j | \xi_i = 1] = \frac{b(b-1)}{n(n-1)}.$$

Then we get

$$2 \frac{n(n-1)}{b(b-1)} \sum_{i < j} \mathbb{E}_\xi[\xi_i \xi_j] A_{i,j} u_i^\top u_j = 2 \sum_{i < j} A_{i,j} u_i^\top u_j.$$

Adding the two terms back together, we get the trace term.

### A.2 ADNI IMAGES



(a) Train images

(b) Baseline

(c) Grid Search

(d) Joint

Figure 3: Random samples of ADNI train images and images generated by the normalizing flow models.